Identification of the progenitors of rich clusters and member galaxies in rapid formation at $z > 2$

Rhythm Shimakawa,[1,2]* Tadayuki Kodama,[2,3] Ken-ichi Tadaki,[3] Ichi Tanaka,[1]
Masao Hayashi[4] and Yusei Koyama[3]

[1]*Subaru Telescope, National Astronomical Observatory of Japan, 650 North A'ohōkū Place, Hilo, HI 96720, USA*
[2]*Department of Astronomy, School of Science, Graduate University for Advanced Studies, Mitaka, Tokyo 181-8588, Japan*
[3]*Optical and Infrared Astronomy Division, National Astronomical Observatory, Mitaka, Tokyo 181-8588, Japan*
[4]*Institute for Cosmic Ray Research, The University of Tokyo, Kashiwa, Chiba 277-8582, Japan*

ABSTRACT

We present the results of near-infrared spectroscopy of Hα emitters (HAEs) associated with two protoclusters around radio galaxies (PKS 1138−262 at $z = 2.2$ and USS 1558−003 at $z = 2.5$) with the Multi-Object Infrared Camera and Spectrograph (MOIRCS) on the Subaru telescope. Among the HAE candidates constructed from our narrow-band imaging, we have confirmed membership of 27 and 36 HAEs for the respective protoclusters, with a success rate of 70 per cent of our observed targets. The large number of spectroscopically confirmed members per cluster has enabled us for the first time to reveal the detailed kinematical structures of the protoclusters at $z > 2$. The clusters show prominent substructures such as clumps, filaments and velocity gradients, suggesting that they are still in the midst of rapid construction to grow to rich clusters at later times. We also estimate the dynamical masses of the clusters and substructures, assuming their local virialization. The inferred masses ($\sim 10^{14}$ M$_\odot$) of the protocluster cores are consistent with their being typical progenitors of the present-day most massive class of galaxy clusters ($\sim 10^{15}$ M$_\odot$) if we take into account the typical mass growth history of clusters. We then calculate the integrated star formation rates of the protocluster cores normalized by the dynamical masses and compare these with lower redshift descendants. We see a marked increase of star-forming activities in the cluster cores, by almost three orders of magnitude, as we go back in time to 11 billion years ago; this scales as $(1 + z)^6$.

Key words: galaxies: clusters: general – galaxies: evolution – galaxies: formation.

1 INTRODUCTION

In protoclusters at $z > 2$, characteristic relations seen in low-z clusters ($z < 1$), such as the colour–magnitude relation, break down as galaxies enter into their formation phase (Kodama et al. 2007). Since the galaxies in those protoclusters are destined to evolve into early-type galaxies in rich clusters today, the protoclusters provide us with unique laboratories in which to investigate directly the formation mechanisms of early-type galaxies and their environmental dependence, through comparison with field galaxies at similar redshifts. It is therefore essential to investigate the characteristics of protoclusters at $z > 2$ systematically, in order to know how star-forming (SF) activities in high-density regions at high z are intrinsically biased and how they are affected externally by their surrounding environments to establish the strong environmental dependence seen in the present-day Universe.

With this motivation, we have been conducting a systematic study of protoclusters at $z > 1.5$ with Subaru as the project 'Mapping HAlpha and Lines of Oxygen with Subaru' (Mahalo–Subaru: for more details see Kodama et al. 2013). We have conducted narrow-band (NB) imaging with many customized NB filters and have successfully identified Hα or [O II] emitter candidates that are physically associated with the protoclusters. The following two objects are among the richest systems ever identified: USS 1558−003 at $z = 2.53$ (Hayashi et al. 2012, hereafter H12) and PKS 1138−262 at $z = 2.16$ (Koyama et al. 2013, hereafter K13). Since they both show large excesses in number densities of SF galaxies, these protoclusters are probably still in the vigorous formation process. Our observations have revealed high SF activities towards the cores of protoclusters at $z > 2$. The peak of SF activity traced by the line emitters is shifted from dense cluster cores to lower density outskirts and filamentary outer structures with time from $z \sim 2.5$ to $z \sim 0.4$, indicating the inside-out growth of clusters.

*E-mail: rhythm.shimakawa@nao.ac.jp

These results are all intriguing, but we need to confirm them and investigate the physical properties of protocluster galaxies in much greater detail with spectroscopic follow-up observations. This Letter reports the first results of our near-infrared (NIR) spectroscopy of HAEs in the two richest protoclusters at $z > 2$. We first describe our targets and the method of spectroscopic observations and then present the kinematical structures of spectroscopically confirmed members. We also discuss SF activities in these two systems through comparison with lower redshift counterparts. We assume a Λ-dominated cosmology with $\Omega_M = 0.3$, $\Omega_\Lambda = 0.7$ and $H_0 = 70$ km s^{-1} Mpc^{-1}.

2 OBSERVATION AND DATA REDUCTION

Our targets are selected on the basis of NB Hα imaging together with broad-band imaging of the two protoclusters around the radio galaxies (RGs), namely PKS 1138$-$262 ($z = 2.16$) and USS 1558$-$003 ($z = 2.53$), hereafter PKS 1138 and USS 1558, respectively. First we sample line emitters that show excess fluxes in the narrow-band and then use a broad-band colour–colour diagram (BzK or rJK) to separate Hα emitters at the cluster redshift from contaminant [O III]/[O II]/Paα emitters at other redshifts (see K13 and H12 for more details). We select the emitters with Hα fluxes larger than 2.5×10^{-17} erg s^{-1} cm^{-2} as estimated from the NB imaging (K13; H12), which corresponds to SFR ~ 19–25 M$_\odot$ yr^{-1} for PKS 1138 and USS 1558, respectively, using the Kennicutt (1998) conversion. We have identified 48 and 68 HAEs candidates in the vicinity of PKS 1138 and USS 1558 respectively (K13; H12). We used the Multi-Object Infrared Camera and Spectrograph (MOIRCS), a NIR imager and spectrograph (Ichikawa et al. 2006; Suzuki et al. 2008) mounted on the 8.2-m Subaru Telescope on Mauna Kea. It provides a multi-object spectroscopic (MOS) capability at ~ 0.9–2.5 μm with a 4×7 arcmin^2 field of view covered by two *HAWAII-2* 2048 $\times$ 2048 arrays with the spatial resolution of 0.117 arcsec pixel^{-1}. We used a low-resolution grism (HK500: $R \sim 500$ for 0.8 arcsec slit width) for 5 masks and a high-resolution grism (VPH-K: $R \sim 1700$ for 0.8 arcsec slit width; see Ebizuka et al. 2011) for one of the 3 masks for PKS 1138. We made more than 15 slits per mask. In total, 98 objects were observed (some targets were redundant).

We spent 5 nights (March–April in 2013) under 0.6–1 arcsec seeing conditions for most of the time; however, one night was completely lost due to bad weather. The net integration times were longer than 2 h per mask. A summary of the observations is given in Table 1.

Table 1. Summary of the observations. Columns: (1) cluster name, (2) grism name, (3) resolution with 0.8 arcsec slit width, (4) integration time and (5) the number of observed targets. HK500 and VPH-K indicate low- and high-resolution grisms covering the ranges 1.3–2.5 and 1.9–2.3 μm, respectively.

Cluster Name (1)	Grism (2)	R (3)	Integ. time (4)	Targets (5)
PKS 1138$-$262	HK500	513	120 min	23
(11:40:48,$-$26:29:08)	HK500	513	161 min	19
$z = 2.16$	VPH-K	1675	225 min	18
USS 1558$-$003	HK500	513	180 min	25
(16:01:17,+00:28:48)	HK500	513	276 min	19
$z = 2.53$	HK500	513	175 min	15

Data reduction was carried out using the MOIRCS MOS Data Pipeline (MCSMDP;[1] Yoshikawa et al. 2010) which is a data reduction package based on IRAF[2] for spectroscopic data of MOIRCS. This pipeline executes bad pixel masking, cosmic-ray rejection, pairwise frame subtraction, correction for distortion and the combination of positive and negative spectra semi-automatically. A wavelength calibration is performed with OH lines and a flux calibration is performed using standard stars with a spectral type of A0V. For USS 1558, we checked the result of wavelength calibration carefully by comparing it with thorium argon lines, since Hα lines are located beyond $\lambda = 2.3$ μm, where there is no remarkable OH line. However, it should be noted that since thorium argon lines are not strong enough at the long wavelength range of 2.3–2.5 μm, we have larger uncertainties for the USS 1558 members. Therefore we use an [O III] emission line, if available, to estimate the redshift of a USS 1558 member. The root-mean-square error (RMS) of wavelength calibration is about ± 3Å, which corresponds to ± 40–50 km s^{-1}. This error is negligible for determination of the velocity dispersion of each cluster.

3 RESULTS

We first search for emission lines in the wavelength range of NB filters, where Hα line candidates have already been detected by past NB imaging surveys. Next they are fitted by Gaussian curves with SPECFIT (Kriss 1994), which is distributed within STSDAS[3] layered on top of the IRAF environment. We normally apply a single Gaussian fitting, but sometimes a multi-Gaussian fitting for a broad or multiple emission line, and the chi-square minimization technique is used to best fit the line profile. Further details of the line fitting will be presented in our forthcoming full Paper II (in preparation).

In the obtained spectra, we identified one or more new emission lines at above 3σ levels for 27 and 36 SF galaxies in PKS 1138 and USS 1558 clusters, respectively. Here, the 1σ threshold is defined as a standard deviation of flux densities around each emission line, excluding the line itself. The limiting magnitude of this spectroscopy (1σ) is $m_{AB} = 22.2$–22.6 in the K band. The completeness of our observation is 76 per cent (90 observed out of 116 candidates) and the efficiency or success rate is 70 per cent (63 confirmed out of 90 observed). A summary of our spectroscopic confirmations is presented in Table 2. We note that velocity dispersions and R_{200} are measured including the cluster members reported in past studies. The histograms (Fig. 1) show the redshift distributions of HAEs in the two protoclusters. For PKS 1138, we also plot cluster members identified by past works (Kurk et al. 2000, 2004; Croft et al. 2005; Doherty et al. 2010) and in total 49 members have been spectroscopically confirmed, including the RG.

It should be noted that a relatively strong OH sky line is located at $\lambda = 2.073$ nm and this significantly affects our line detectability at the specific redshift interval $z = 2.156$–2.162 for the Hα emission line. This actually contributes to the dip seen in the redshift distribution at the corresponding bin. The velocity dispersions of 'PKS 1138 all' and 'PKS 1138 C1' shown in Table 2 may decrease by 20–30 km s^{-1} if we take this effect into account.

As seen in Fig. 1, cluster members are mostly located at redshifts where the response curve has maximum sensitivity. The large

Table 2. Summary of spectroscopic confirmations. Columns: (1) cluster name as shown in Fig. 2, (2) newly confirmed number of members, (3) mean peculiar velocity, (4) velocity dispersion, (5) R_{200} and (6) cluster mass (M_{cl}) calculated from Finn et al. (2005).

Cluster name (1)	New members (2)	$\langle \Delta V \rangle$ [km s^{-1}] (3)	σ_{cl} [km s^{-1}] (4)	R_{200} [Mpc] (5)	M_{cl} [10^{14} M$_\odot$] (6)
PKS 1138 all	27	−41	882^a	—	—
PKS 1138 C1	9	+9	683^a	0.53^a	1.71^a
USS 1558 all	36	−717	756	—	—
USS 1558 C1	7	+121	284	0.19	0.10
USS 1558 C2	19	−1042	574	0.38	0.87

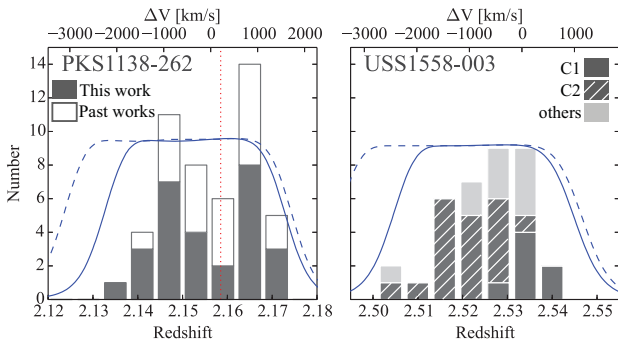^{a}Estimated including Lyα emitters in the literature.

Figure 1. Distribution of redshifts and peculiar velocities with respect to the RGs in PKS 1138 (left) and USS 1558 clusters (right). Blue solid curves show the response curves of the NB filters used in K13 and H12, namely NB2071 ($\lambda_c = 2.070$ μm, FWHM = 0.027 μm) and NB2315 ($\lambda_c = 2.317$ μm, FWHM = 0.026 μm); both of the two filters belong to T. Kodama. Blue dashed curves represent the range of wavelength shifts of the transmission curves within the FoV.[4] Left: black and white histograms present our results (including the RG) and those of past works (Kurk et al. 2000, 2004; Croft et al. 2005; Doherty et al. 2010). The red dotted line indicates the location of a strong OH line at λ = 2.073 nm. Right: confirmed cluster members including the RG are plotted. Black solid, slashed and grey solid histograms show the galaxies in clumps 1, 2 and outside them in the protocluster, respectively. The bin size is $\Delta z = 0.006$ in both panels. The top axis shows peculiar velocities (ΔV) with respect to each RG.

numbers of newly confirmed members in both clusters have confirmed that these systems are indeed rich protoclusters hosting lots of highly SF young galaxies with typical star formation rates (SFRs) of ∼15–800 M$_\odot$ yr^{-1} after dust extinction correction. Since they are widespread and show clear substructures, as shown in Fig. 2, the protoclusters are right in the phase of vigorous assembly. It should be noted, however, that only 15 and 21 galaxies out of 27 and 36 emitters in PKS 1138 and USS 1558, respectively, are confirmed with detections of more than one emission line. Although our colour selection works well to discriminate between Hα lines at the cluster redshifts and other contaminant lines at the wrong redshifts (K13; H12), we cannot fully rule out some contamination from the fore- or background of the protoclusters. In fact, we identified one background [O III] emitter with doublet lines in each field. Therefore, among those 38 targets with redshifts determined with multiple lines, 36 were identified as HAEs at the cluster redshifts.

The contamination level by fore- or background galaxies would then be ∼5 per cent and thus has little impact on the current study.

4 DISCUSSION AND CONCLUSIONS

Kinematical structures of distant protoclusters provide essential information on the mass assembly history of galaxy clusters. Fig. 2 presents the spatial and redshift (or radial velocity) distributions of the HAEs (and 15 confirmed LAEs in the case of PKS 1138). The blue and red symbols separate the members according to their redshifts or radial velocities: those approaching or receding, respectively, with respect to the radio galaxies.

From the velocity dispersion, we now estimate R_{200} for each protocluster, which is the radius within which the averaged matter density is 200 times larger than the critical density. The dynamical mass of each system (M_{cl}) is also measured using the virial theorem (Finn et al. 2005), assuming local virialization.

4.1 PKS 1138−262 (z = 2.16)

PKS 1138 is among the most familiar protoclusters at $z \sim 2$ and has been intensively studied by many researchers (e.g. Kurk et al. 2000).

We see some velocity structures across the protocluster (Fig. 2a) as well as the spatial structure. The galaxies near the RG within the dashed circle denoted as C1 seem to be relatively well mixed in velocity. However, the outer region is more structured. The most prominent structure is a linear filament extending towards the southeast direction from the RG. This almost perfectly aligned filament is dominated by approaching galaxies with respect to the RG, suggesting that those galaxies are falling on to the protocluster core along the filament and penetrating into the very centre. On the other hand, the north-west and east areas are preferentially occupied by receding populations. The south-west complex further away from the protocluster centre near the bottom right corner of the figure consists solely of approaching galaxies, suggesting the existence of a coherently moving group or filament.

All these spatial and kinematic structures seem to suggest that the inner part of the cluster centred on the RG (<0.5 Mpc) is already collapsed and nearly virialized, while the outer regions are still highly structured and are at the early phase of assembly towards the protocluster core. The radio galaxy PKS 1138 is right at the junction of the infalling filaments at the dynamical centre.

Upon the assumption of virialization in the core, the dynamical mass of the core is estimated at 1.71×10^{14} M$_\odot$ from the velocity dispersion of 683 km s^{-1} within C1. X-ray observations of this system with the High Resolution Imager on *ROSAT* show that the emitted energy is $6.7 \pm 1.3 \times 10^{44}$ erg s^{-1} in the 2–10 keV band, corresponding to the dynamical mass of $\sim 10^{14}$ M$_\odot$. It is consistent with our result, although the X-ray emission is contaminated by active galactic nuclei (Carilli et al. 1998; Pentericci et al. 2002).

4.2 USS 1558−003 (z = 2.53)

USS 1558 is the densest protocluster ever known to date at $z > 2$ and was first discovered by Kajisawa (2006) and H12. H12 identified three groups of HAEs aligned along the north-east–south-west directions: a loose group around the RG, the richest clump at 3.5 arcmin away from the RG and a small clump in between the two. This work revises that previous grouping to two clumps C1 and
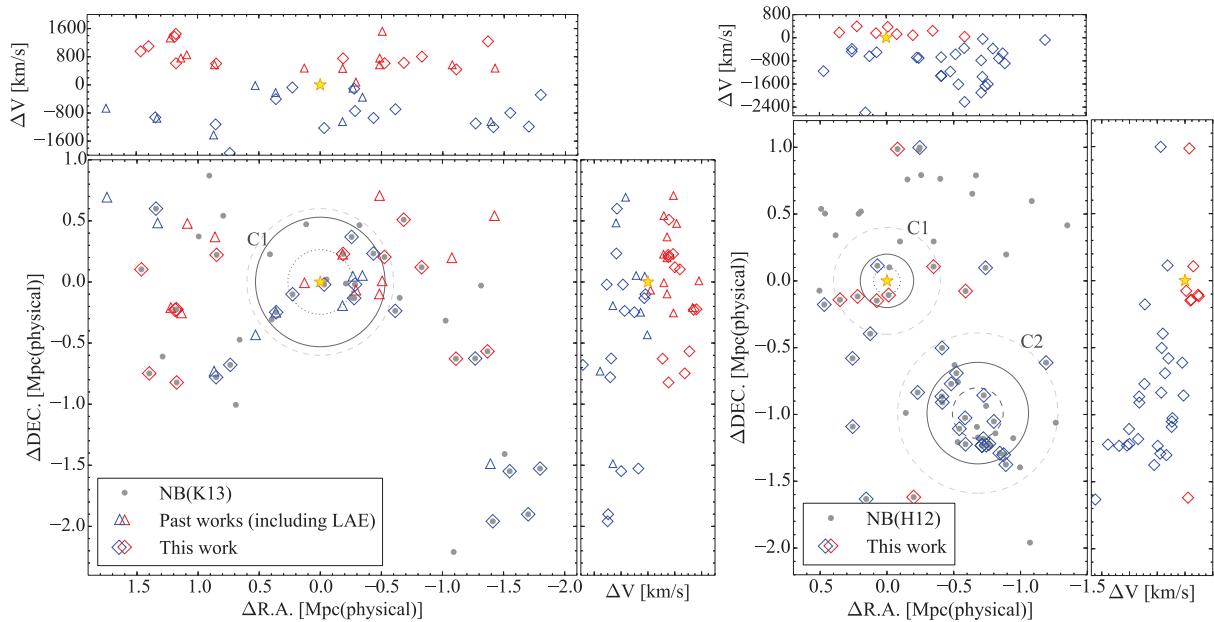
Figure 2. The kinematical structures of HAEs in PKS 1138 (left) and USS 1558 clusters (right). Grey dots represent HAE candidates detected in our NB imaging (K13 and H12). Diamonds show the members newly confirmed in this study. Triangles are the confirmed Hα and Lyα emitters (LAE) in the previous works (Kurk et al. 2000, 2004; Croft et al. 2005; Doherty et al. 2010). Blue and red symbols are separated by blue- and redshifted galaxies, respectively, relative to the RGs (star mark). We identify three groups, namely PKS 1138-C1, USS 1558-C1 and USS 1558-C2, and they are shown by grey dashed circles. Solid and dotted black circles indicate R_{200} and $0.5 \times R_{200}$, respectively.

C2 as shown in Fig. 2(b) because of the poor kinematical separation between the latter two clumps, identified only spatially in the previous study. We have now confirmed spectroscopically that the two groups are actually located at the redshift of the RG and are embedded in the large-scale structure. C2 is particularly rich, as it confines 19 spectroscopically confirmed HAEs and 12 more candidates (not confirmed yet) within a radius of 0.6 Mpc and is the densest system ever identified at high redshifts ($z > 2$). We note that the RG itself seems to be offset from this densest clump, unlike the PKS 1138 cluster.

Judging from the very high densities of the HAEs in compact areas, we could reasonably assume a local virialization in these regions and the corresponding dynamical masses and R_{200} are estimated and listed in Table 2. The dynamical mass of C2 is estimated at 0.87×10^{14} M$_\odot$ from its velocity dispersion of 574 km s^{-1}.

We find that there is a large-scale velocity gradient across the cluster in the direction of the group alignment (north-east–south-west). The velocity distribution and central value of the south-west group (C2) are blueshifted from those of the north-east group (C1) that hosts the RG (Fig. 2; see also Table 2). Therefore those groups are probably physically aligned and gravitationally pulling each other closer. They would eventually merge together and become a single rich cluster in the near future.

4.3 Cosmic evolution of $\Sigma SFR/M_{cl}$

Finally, we investigate the cosmic SF history in galaxy clusters represented by the integrated SFR (ΣSFR) normalized by cluster dynamical mass (Fig. 3a). In order to compare our results directly with the previous works compiled by Finn et al. (2005), we sum up individual SFRs of the Hα (or [O II]) emitters within $0.5R_{200}$, including the candidates whose membership has not been confirmed yet. In this work, we calculate ΣSFR and M_{cl} for the main body of the PKS 1138 cluster (C1) and the richest clump of the USS 1558

cluster (C2), respectively. We assume a uniform dust extinction of $A_{H\alpha} = 1$ and $A_{[O II]} = 1.76 A_{H\alpha}$. To evaluate the uncertainties from this assumption, we also estimate ΣSFR within R_{200}, employing the mass-dependent correction for dust extinction (Garn & Best 2010). Although the absolute values of ΣSFR may have large systematic errors, due to various factors such as sampling bias, active galactic nucleus contribution and so on, the relative differences among different clusters that we see here are more reliable. Koyama et al. (2010, 2011) found that $\Sigma SFR/M_{cl}$ in cluster cores increases dramatically to $z \sim 1.5$ and scales as $\sim(1 + z)^6$ (see also Smail et al. 2014). We find that this trend extends to even higher redshifts to $z \sim 2.5$, as our values of $\Sigma SFR/M_{cl}$ within R_{200} estimated in this work seem to more or less follow the extrapolated curve of the redshift evolution.

In such comparisons of clusters at different redshifts, we must be sure that we are comparing the right ancestors with the right descendants. In fact, clusters grow in mass with cosmic time by a large factor and therefore we should compare galaxy clusters taking into account such mass growth. Fig. 3(b) shows cluster masses as a function of redshift. The red line and the pink zone show the mass growth history of massive cluster haloes predicted by cosmological simulations (Shimizu et al. 2012; Chiang et al. 2013). The data points show the measurements of the dynamical masses of real clusters used for comparison. It turns out that our protoclusters at $z > 2$ have large enough masses to be consistent with the progenitors of the most massive class of clusters, like Coma. The lower-z clusters, shown with filled squares, also follow the same mass growth curve. Therefore we argue that we are comparing the right ancestors with the right descendants and the redshift variation of the mass-normalized SFRs seen in the upper panel can be seen as the intrinsic cosmic SF history of the most massive class of clusters.

In this Letter, we have presented the kinematical structures of the two richest protoclusters at $z > 2$ and extended the cosmic evolution
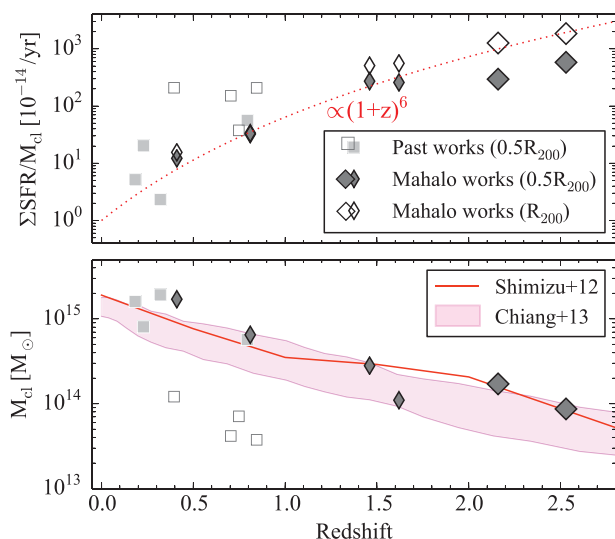
Figure 3. (a) Integrated SFRs in the cluster cores, ΣSFR, normalized with cluster dynamical masses (upper panel) and (b) cluster dynamical masses (lower panel) are plotted as a function of redshift. The open diamonds show the measurements for the Mahalo–Subaru cluster sample including this work, calculated within R_{200} of each cluster (Koyama et al. 2010, 2011; Hayashi et al. 2011; Tadaki et al. 2012). The filled diamonds indicate the values within $0.5R_{200}$, to match the definition with other previous measurements for a direct comparison. The previous works for eight clusters at $z = 0.1$–0.9 are shown by squares (compilation by Finn et al. 2005). The grey and open squares separate those clusters according to their dynamical masses, as shown in the lower panel. Note that SFRs are measured from Hα line strengths for all the clusters except for the $z = 1.46$ and $z = 1.62$ clusters, which are based on [O II] lines. Note also that R_{200} is not fully covered for the $z = 0.81$ cluster. The cluster mass of the J0218 cluster at $z = 1.62$ is adopted from Tanaka, Finoguenov & Ueda (2010). The red dotted curve shows the relation as a function of redshift, scaling as $(1 + z)^6$. In the lower panel, the red line and the pink zone show the typical mass growth history of massive cluster haloes with 1–2×10^{15} M$_\odot$ predicted by theoretical models (Shimizu, Yoshida & Okamoto 2012; Chiang, Overzier & Gebhardt 2013). The pink zone corresponds to $\pm 1\sigma$ scatter around the median values.

of ΣSFR/M_{cl} back to $z > 2$ or 11 Gyr ago, based on intensive multi-object NIR spectroscopy of the NB-selected star-forming galaxies. In our forthcoming Paper II (in preparation), we will discuss the physical properties of these galaxies (such as gaseous metallicities, ionizing states and dust extinction) using multi-emission-line diagnostics and compare them with those in the general field at similar redshifts.

REFERENCES

Carilli C. L., Harris D. E., Pentericci L., Röttgering H. J. A., Miley G. K., Bremer M. N., 1998, ApJ, 494, L143
Chiang Y.-K., Overzier R., Gebhardt K., 2013, ApJ, 779, 127
Croft S., Kurk J. D., van Breugel W., Stanford S. A., de Vries W., Pentericci L., Röttgering H. J. A., 2005, AJ, 130, 867
Doherty M. et al., 2010, A&A, 509, 83
Ebizuka N. et al., 2011, PASJ, 63, 605
Finn R. A. et al., 2005, ApJ, 630, 206
Garn T., Best P. N., 2010, MNRAS, 409, 421
Hayashi M., Kodama T., Koyama Y., Tadaki K.-i., Tanaka I., 2011, MNRAS, 415, 2670
Hayashi M., Kodama T., Tadaki K.-i., Koyama Y., Tanaka I., 2012, ApJ, 757, 15
Ichikawa T. et al., 2006, SPIE, 6269, 38
Kajisawa M., Kodama T., Tanaka I., Yamada T., Bower R., 2006, MNRAS, 371, 577
Kennicutt R. C., Jr1998, ARA&A, 36, 189
Kodama T., Tanaka I., Kajisawa M., Kurk J., Venemans B., De Breuck C., Vernet J., Lidman C., 2007, MNRAS, 377, 1717
Kodama T., Hayashi M., Koyama Y., Tadaki K.-i., Tanaka I., Shimakawa R., 2013, in Thomas D., Pasquali A., Ferreras I., eds, Proc. IAU Symp. 295, Mahalo-Subaru: Mapping Star Formation at the Peak Epoch of Massive Galaxy Formation. Cambridge Univ. Press, Cambridge, p. 74
Koyama Y., Kodama T., Shimasaku K., Hayashi M., Okamura S., Tanaka I., Tokoku C., 2010, MNRAS, 403, 1611
Koyama Y., Kodama T., Nakata F., Shimasaku K., Okamura S., 2011, ApJ, 734, 66
Koyama Y., Kodama T., Tadaki K.-i., Hayashi M., Tanaka M., Smail I., Tanaka I., Kurk J., 2013, MNRAS, 428, 1551
Kriss G., 1994, Astronomical Data Analysis Software and Systems, 3, 437
Kurk J. D. et al., 2000, A&A, 358, L1
Kurk J. D., Pentericci L., Overzier R. A., Röttgering H. J. A., Miley G. K., 2004, A&A, 428, 817
Pentericci L., Kurk J. D., Carilli C. L., Harris D. E., Miley D. K., Röttgering H. J. A., 2002, A&A, 396, 109
Shimizu I., Yoshida N., Okamoto T., 2012, MNRAS, 427, 2866
Smail I. et al., 2014, ApJ, 782, 19
Suzuki R. et al., 2008, PASJ, 60, 1347
Tadaki K.-i. et al., 2012, MNRAS, 423, 2617
Tanaka M., Finoguenov A., Ueda Y., 2010, ApJ, 716, L152
Yoshikawa T. et al., 2010, ApJ, 718, 112

This paper has been typeset from a TEX/LATEX file prepared by the author.